manuscript accepted in *Paleoceanography* (https://doi.org/10.1029/2024PA004968)

Carbon cycle and circulation change in the North Pacific Ocean at the initiation of Northern Hemisphere Glaciation constrained by boron-based proxies in diatoms

H. K. Donald[1], G. E. A. Swann[2], J. W. B. Rae[3] and G. L. Foster[1]

[1]School of Ocean and Earth Science, National Oceanography Centre Southampton, University of Southampton, Southampton, SO14 3ZH, UK.

[2]School of Geography, University of Nottingham, University Park, Nottingham, NG7 2RD, UK.

[3]School of Earth and Environmental Sciences, University of St Andrews, St Andrews KY16 9AL, UK. (Affiliations should be preceded by superscript numbers corresponding to the author list. Each affiliation should be run in so that the full affiliation list is a single paragraph.)

Corresponding author: George Swann (george.swann@nottingham.ac.uk)

Key Points:

- $\delta^{11}B$ and [B] in diatom frustules reveal a surface water increase of 0.3 to 0.5 pH units in the subarctic Pacific Ocean over the iNHG.
- These changes would have lowered atmospheric pCO_2 and contributed to the long-term expansion of Northern Hemisphere ice-sheets.

Abstract

The intensification of Northern Hemisphere glaciation (iNHG) at 2.73 Ma is associated with a reorganization of the subarctic Pacific Ocean and abrupt drop in opal mass accumulation rates. Uncertainty, however, remains around the extent to which these changes altered carbon dynamics and contributed to a reduction in atmospheric pCO_2 and global temperatures. These issues are addressed here using the boron isotope ($\delta^{11}B$) proxy in diatom frustules to reconstruct past changes in the pH and pCO_2 of ambient seawater. Diatom $\delta^{11}B$ and [B] indicate a subarctic Pacific surface water increase of 0.3 to 0.5 pH units over the iNHG. This confirms that delivery of carbon and nutrients into surface waters was reduced at this time, explaining the drop in opal productivity and limiting CO_2 outgassing from the ocean interior. We consider two hypotheses to explain this based on potential changes in circulation from the late Pliocene to early Pleistocene: "ventilation to stratification" or "stratification to ventilation". The ventilation to stratification hypothesis, which posits a switch from vigorous PMOC in the Pliocene to stratification over iNHG, has received more attention in the literature. The stratification to ventilation hypothesis, which posits a modest increase in ventilation, is more consistent with modern and late Pleistocene analogues, the majority of models and $\delta^{13}C$ data. These late Pliocene changes in the subarctic Pacific, in conjunction with other external and internal processes including those in the Southern Ocean, would have contributed to a lowering of atmospheric pCO_2 and the long-term expansion of ice-sheets across the Northern Hemisphere.

1 Introduction

Under current shared socio-economic pathways (SSP), atmospheric CO_2 concentrations ($pCO_{2(atm)}$) by 2100 CE will range from 393 ppm (SSP1-1.9) to 1,135 ppm (SSP5-8.5) (Meinshausen et al. 2020). Due to the absence of comparable intervals within the observational record, the geological record becomes crucial in efforts to constrain how the Earth system might respond to increased CO_2 forcing, including the reorganizations of ocean-atmospheric processes (Tierney et al 2020). Of equal importance is the need to consider future tipping points under a warmer climate state (Wunderling et al 2021), the detection of which can be achieved through the study of natural ("paleo") archives (Thomas, 2016). One of the most significant of these in the recent geological past is the intensification of Northern Hemisphere Glaciation (iNHG) from 2.73 Ma, when the Earth system transitioned from a relatively warm and climatological stable Pliocene to the unstable Quaternary characterized by orbitally-paced oscillations between glacial and interglacial states (McClymont et al., 2023). Coincident with the iNHG and the appearance of large continental ice sheets over northern Eurasia and North America (Kleiven et al 2002; Tan et al., 2018) are a series of step-like transitions across both atmospheric and oceanic meridional temperature gradients (Brierley and Fedorov, 2010; McClymont et al., 2023) and circulation patterns (Sato et al 2015; Abell et al., 2021). These includes a series of changes associated with the reorganization of the subarctic Pacific Ocean, which may have sufficiently altered regional carbon dynamics to impact the long-term global climatic cooling that occurred over this interval (Haug et al., 1999).

Key changes observed in proxy data from the subarctic Pacific at 2.73 Ma include a drop in sediment opal (Haug et al., 1999) and calcium carbonate content (Haug et al., 1995; Burls et al., 2017), accompanied by an increase in nitrogen isotope ratios (Haug et al., 1999; Sigman et al., 2004; Studer et al., 2012). Together, these signals imply a reduction in the supply of nutrients

to the surface ocean. As oceanic nutrient and carbon concentrations are largely coupled, these changes have been interpreted to imply a reduction in CO_2 outgassing from the subarctic Pacific around the iNHG, potentially helping to lower atmospheric CO_2 and contributing to global cooling and ice sheet growth (Haug et al., 1999, 2005). However, several potential uncertainties remain. For instance, nitrogen isotopes can be influenced by water column denitrification, in addition to nutrient utilization, potentially complicating the interpretation of North Pacific $\delta^{15}N$ signals (e.g. Galbraith et al., 2008), while CO_2 is not always straightforwardly coupled with nutrients, for instance due to changes in air sea gas exchange. More direct records of surface ocean CO_2 chemistry could help address these issues and improve our understanding of what happened to the subarctic Pacific Ocean CO_2 system during the iNHG.

Over the past decade significant information on atmospheric CO_2 and the oceanic carbon system has been obtained using boron isotopes ($\delta^{11}B$) in foraminifera (e.g. Foster and Rae, 2016; Hönisch et al., 2019; Rae et al. 2021; CenCO2PIP Consortium, 2023). However, due to the rarity of carbonate microfossils in subarctic Pacific Ocean sediments, such analyses are not possible in this region. Building on recent method development and culturing calibrations (Donald et al. 2020), we provide here the first diatom $\delta^{11}B$ ($\delta^{11}B_{diatom}$) and B concentration ($[B]_{diatom}$) paleoceanographic record to constraint how surface pH, carbon dynamics and hence air-sea CO_2 flux in the subarctic Pacific Ocean responded to changing oceanographic conditions over the iNHG.

2 Materials and Methods

2.1 ODP Site 882

ODP Site 882 is situated at the western section of the Detroit Seamounts (50°220N, 167°360E) in the open waters of the northwest Pacific Ocean at a water depth of 3,244 m (Fig. 1). The modern water column around ODP Site 882 is characterized by a highly stable year-round halocline stratification at ca. 100 – 150 m water depth, with surface waters of ca. 32.8 psu (Zweng et al., 2018). From June to October, this stratification is then strengthened by a thermocline at ca. 50 m with sea surface temperatures (SST) of ca. 8–11°C (Locarnini et al., 2018). Modern values of surface water CO_2 concentrations ($pCO_{2(aq)}$) in the region (50°–50.5°N and 167°–168°E) over the past two decades and across different seasons range from 331–408 µatm (Takahashi et al., 2016). Monthly differences between $pCO_{2(aq)}$ and $pCO_{2(atm)}$ of overlying air (ΔpCO_2) range from −50 to +44 µatm, whilst modern annual mean and preindustrial mean ΔpCO_2 are close to 0 µatm (Takahashi et al., 2009; Japan Agency for Marine-Earth Science and Technology et al., 2013). When compared to the North Atlantic, the North Pacific shows higher $pCO_{2(aq)}$ and lower pH (Fig. 1).

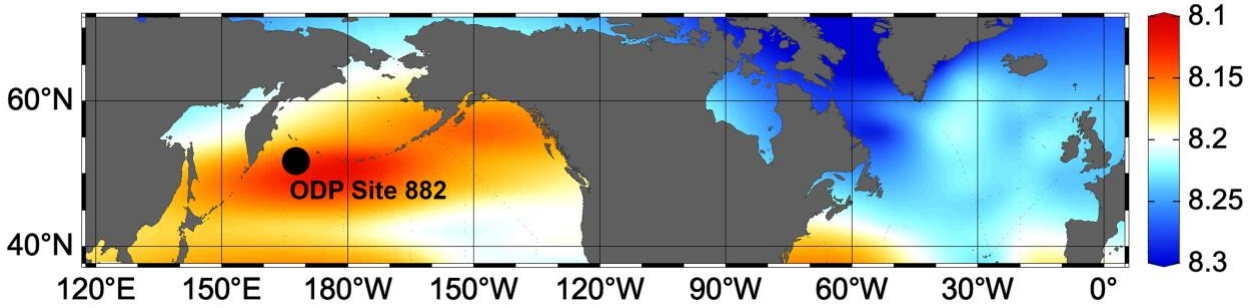

Figure 1. Location of ODP Site 882 (50°220N, 167°360E) in the northwest subarctic Pacific

Ocean. Colors indicate annual modern gridded surface water pH from GLODAP, corrected for the influence of anthropogenic carbon (Olsen et al., 2020). Map created using Ocean Data View (https://odv.awi.de). Upwelling of carbon-rich deep waters in the modern stratified North Pacific Ocean creates relatively acidic surface waters, rich in CO_2. Conversely, the North Atlantic Ocean is fed by carbon and nutrient-depleted waters from the subtropics, which are then flushed to depth via an active overturning circulation.

2.2 Boron in diatoms

Boron is bound to oxygen in either a tetrahedral (e.g. borate ion such as $B(OH)_4^-$) or a trigonal (e.g. boric acid such as $B(OH_3)$ complex, with the concentration of boron in seawater $[B]_{sw}$:

$$[B]_{sw} = [B(OH)_4^-] + [B(OH)_3] \qquad (1)$$

The abundance of individual boron species are then linked by the acid-base equilibrium:

$$[B(OH)_4^-] + H^+ <=> [B(OH)_3] + H_2O \qquad (2)$$

Boron has two stable isotopes ^{10}B (~20%) and ^{11}B (~80%), the isotope ratio of which is expressed as $\delta^{11}B$:

$$\delta^{11}B(‰) = \left(\frac{^{11}B/^{10}B_{sample}}{^{11}B/^{10}B_{standard}} - 1\right) \bullet 1000 \qquad (3)$$

where $^{11}B/^{10}B_{standard}$ is the boron isotopic composition of National Institute of Standards and Technology (NIST) Standard Reference Material (SRM) 951 boric acid ($^{11}B/^{10}B$=4.04367; Catanzaro et al. 1970). Due to boron's long residence time (10–20 Myr; Lemarchand et al. 2002), boron is well mixed in the ocean with the isotopic composition of seawater ($\delta^{11}B_{sw}$) being 39.61 ± 0.04‰ (Foster et al. 2010). There is then an isotopic fractionation between $B(OH)_3$ and $B(OH)_4^-$ of ~27 ‰ (Klochko et al. 2006; Nir et al 2015) with ^{11}B preferentially incorporated into the more strongly bonded trigonal molecule $B(OH)_3$:

$$^{10}[B(OH)_3] + {}^{11}[B(OH)_4^-] <=>^{11} [B(OH)_3] + {}^{10}[B(OH)_4^-] \qquad (4)$$

Since the concentration and isotopic ratios of boron species are altered by pH (Equation 2) but must sum to $[B]_{sw}$ and $\delta^{11}B_{sw}$, the isotopic composition of $B(OH)_3$ and $B(OH)_4^-$ (expressed as $\delta^{11}B$) also varies with pH. Given that it is predominantly the charged $B(OH)_4^-$ species that is incorporated into growing $CaCO_3$, the $\delta^{11}B$ of marine carbonates can be used to constrain past changes in pH and so marine/global carbon dynamics (Fig. 2; Hemming and Hanson, 1992; Zeebe and Wolf-Gladrow, 2001; Foster and Rae, 2016). For example, $\delta^{11}B$ has been widely used in foraminiferal carbonates to reconstruct ocean pH and atmospheric pCO_2 across a variety of timescales (e.g. Hemming and Hanson, 1992; Pearson and Palmer, 2000; Hönisch and Hemming, 2005; Foster, 2008; Henehan et al., 2013; Chalk et al., 2017; CenCO2PIP Consortium, 2023).

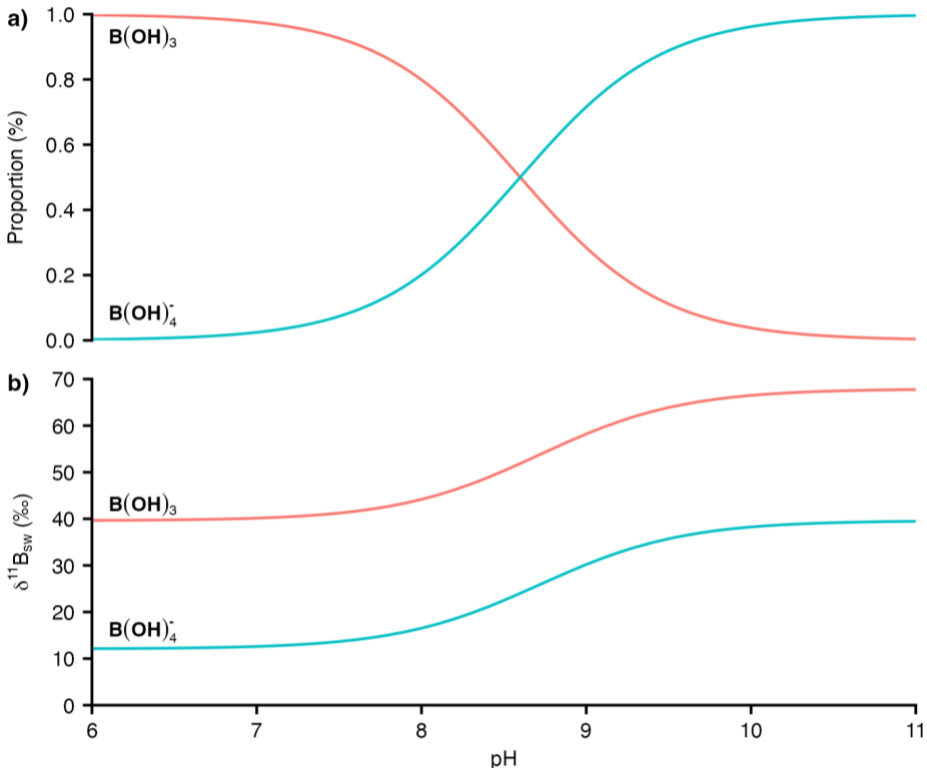

Figure 2. Variation in seawater concentrations (a) and isotopic composition (b) of $B(OH)_4^-$) and $B(OH_3)$ with pH using surface seawater conditions of 25°C and 34.7 psu.

Earlier work on biogenic silica sediment samples from the equatorial and North Pacific Ocean demonstrated relatively high [B] concentrations (70–80 ppm) and low $\delta^{11}B$ values (diatoms = −1.1‰, radiolaria = +4.5‰ [Ishikawa and Nakamura, 1993]; cherts = −9.3‰ to +8‰ [Kolodny and Chaussidon, 2004]). However, diagenetic processes may have altered cherts $\delta^{11}B$ whilst low diatom and radiolaria $\delta^{11}B$ values may indicate clay contamination (Ishikawa and Nakamura, 1993). More recent work on diatom cultures (*Thalassiosira pseudonana* and *Thalassiosira weissflogii*) have shown $[B]_{diatom}$ of 1–10 ppm, with $[B]_{diatom}$ increasing and $\delta^{11}B_{diatom}$ decreasing as pH increased from 7.5 to 8.7 (Mejía et al., 2013; Donald et al., 2020). This relationship was interpreted to suggest the seawater tetrahydroxyborate anion (borate; $B(OH)^-_4$) is predominantly incorporated into the diatom frustule via leakage through bicarbonate transporters during active carbon uptake, rather than boric acid ($B(OH)_3$; Donald et al. 2020; Mejía et al. 2013). In a more recent study, Saldi et al. (2021) identified a large negative isotopic fractionation and the occurrence of both trigonal and tetrahedral boron absorbed onto the amorphous silica surface. If these features are preserved on incorporation of B into opal, they offer at least a partial explanation of the opal $\delta^{11}B$ and B data to date (i.e. Donald et al., 2020), including potentially contributing to the weaker and reversed pH dependency (with respect to expectations based on the aqueous system). While more work is needed to fully understand the mechanisms controlling the boron isotopic signature of siliceous organisms, the negative $\delta^{11}B$-pH relationship shown by Donald et al. (2020) and the positive [B] to pH relationship shown by Mejía et al (2013) and Donald et al. (2020) suggests that $\delta^{11}B_{diatom}$ and $[B]_{diatom}$ represent

potentially useful tracers of paleo-pH and $pCO_{2(aq)}$ in high-latitude marine sediments that have, until now, eluded study due to the lack of suitable carbonate material.

2.3 Diatom sample preparation

The thirty-one samples analyzed in this study for $\delta^{11}B_{diatom}$ and $[B]_{diatom}$ cover the Quaternary/Pliocene boundary from 2.85 - 2.52 Ma and were dated using an age model derived from the astronomical calibration of high-resolution GRAPE density and magnetic susceptibility measurements (Tiedemann & Haug, 1995). All samples are from a 75-150 μm fraction that has previously been extracted for diatom isotopes (see Swann et al., 2006, for full details). In summary, samples were initially wet sieved at 75 μm and 150 μm to both minimize diatom species diversity and remove clays, silts and other non-diatom material. Samples were then immersed in 30% H_2O_2 for up to a week at 80°C to remove organic matter attached to the diatom frustule and later placed overnight in 5% HCl to remove carbonate material. Following centrifuge washing, samples were re-sieved at 75 μm and 150 μm to remove any remaining contamination and smaller diatom, with some samples also requiring the use of a vortex mixer to separate diatoms from contaminants prior to the final sieving stage. Subsamples of the final purified material were mounted on a coverslip using a Naphrax mounting media and visually checked for both contamination and dissolution under a light microscope at 1000 times magnification, with additional checking performed using a scanning electron microscope. These samples have previously been analyzed for diatom $\delta^{13}C$ ($\delta^{13}C_{diatom}$), $\delta^{18}O$ ($\delta^{18}O_{diatom}$) and $\delta^{30}Si$ ($\delta^{30}Si_{diatom}$) (Haug et al., 2005; Swann et al., 2006, 2018; Swann, 2010; Bailey et al., 2011), whilst other work at ODP Site 882 has separately analyzed diatom $\delta^{15}N$ ($\delta^{15}N_{diatom}$ - Studer et al., 2012) and $\delta^{30}Si_{diatom}$ (Reynolds et al., 2008) over the same interval.

2.4 $\delta^{11}B_{diatom}$ and $[B]_{diatom}$ analysis

Sample preparation and analysis for both $\delta^{11}B_{diatom}$ and $[B]_{diatom}$ followed the methodology described in Donald et al. (2020), with an additional set of sample purification steps beyond what was performed when the same samples were analyzed for $\delta^{13}C_{diatom}$, $\delta^{18}O_{diatom}$ and $\delta^{30}Si_{diatom}$ (Swann et al., 2006, 2018; Bailey et al., 2011; Haug et al., 2005; Swann, 2010). This additional stage involved samples being acidified (H_2SO_4), with trace organics then oxidized using a two-step process involving potassium permanganate and oxalic acid (following Horn et al., 2011, and Mejía et al., 2013). Samples were then rinsed using Milli-Q water via centrifugation and transferred to acid-cleaned Teflon beakers. A secondary oxidation was then completed under heat using perchloric acid with organic-free samples rinsed thoroughly with Milli-Q via filtration.

In the boron-free HEPA-filtered class 100 clean laboratory at the University of Southampton, each sample was dissolved completely in a gravimetrically known amount of NaOH (0.5 M from 10 M concentrated stock supplied by Fluka) at 140 ◦C for 48-72 hours. Samples were then briefly centrifuged prior to boron separation to ensure no insoluble particles were loaded onto the boron column. Dissolved samples were passed through an anion exchange column containing Amberlite IRA 743 resin to separate the matrix from the boron fraction following Foster (2008). Samples were loaded directly onto the column without buffering and the matrix removed with 9 × 200 μL washes of Milli-Q. The pure boron fraction was then eluted and collected in 550 μL of 0.5 M HNO_3 acid and a matrix fraction (collected in 1800 μL MilliQ). Potential contamination was monitored using total procedural blanks (TPB) comprising an

equivalent volume of NaOH (0.5 M) and analyzed following the sample analysis protocols detailed below. Typically, the TPBs contained less than 40 pg of boron, equating to a typical blank contribution of ca. 0.015 %. This results in a negligible correction and is therefore not considered further in this work.

Si concentrations of the matrix fraction were determined by having dissolved each opal sample in a known concentration and mass of NaOH and by measuring the Si/Na ratio using a Thermo Scientific X-Series 2 ICP-MS (as detailed in Donald et al., 2020). The Al concentration was also measured on the matrix fraction as a tracer of clay contamination. Prior to isotope analysis, but after column separation, an aliquot (c. 4%) of the boron fraction was diluted 25-fold with 0.5 M HNO_3 and analyzed using a Thermo Fisher Scientific Element 2XR ICP-MS to determine solution [B]. Combining these two sets of analyses ([B] and [Si] of the dissolved sample), and by assuming a chemical formula of $SiO_2.H_2O$ with an H_2O content of 8% (Hendry and Anderson, 2013), the B content of the opal in ppm can be estimated (see Donald et al., 2020). $\delta^{11}B_{diatom}$ was measured on a Thermo Scientific Neptune MC-ICP-MS, also situated in a boron-free HEPA-filtered laboratory at the University of Southampton, following Foster (2008). Instrument-induced fractionation of the $^{11}B/^{10}B$ ratio was corrected using a sample-standard sequence with NIST SRM 951 boric acid, allowing direct determination of $\delta^{11}B$. The reported $\delta^{11}B$ is the mean of the two analyses measured at around 50 ppb [B], with each representing a fully independent measurement. Machine stability and accuracy was monitored using repeats of NIST SRM 951, as well as boric acid reference materials AE120, AE121 and AE122 (also at 50 ppb [B]) that gave $\delta^{11}B$ (±2SD) of −20.19 ± 0.20‰, 19.60 ± 0.28‰ and 39.31 ± 0.28‰, which are within the error of the gravimetric values from Vogl and Rosner (2012). Sample reproducibility was assessed by repeat measurements of an in-house Southern Ocean diatom reference material (TC460) used to develop a method for measuring $\delta^{11}B_{diatom}$ and $[B]_{diatom}$ in Donald et al., (2020). Over the course of this study, on dissolution of TC460 was separated and measured 18 times giving a $\delta^{11}B$ and [B] reproducibility of ± 0.28‰ and ± 20% at 95% confidence, respectively. Through standard addition, Donald et al. (2020) showed that the $\delta^{11}B_{diatom}$ is accurate to ± 0.29‰, and following that study we take the reproducibility of TC460 to be indicative of our accuracy and precision here.

3 Results

3.1 $\delta^{11}B_{diatom}$ and $[B]_{diatom}$

In addition to previous work involving light microscopy and scanning electron microscopy (Swann et al., 2006), a lack of correlation between matrix Al concentrations and $\delta^{11}B_{diatom}$ or $[B]_{diatom}$ confirms the purity of the analyzed diatom samples and the absence of contamination that might alter $\delta^{11}B_{diatom}$ or $[B]_{diatom}$ (Fig. S1). Diatoms in the analyzed 75-150 µm fraction are dominated by two taxa, *Coscinodiscus marginatus* (Ehrenb.) and *Coscinodiscus radiatus* (Ehrenb.). *C. marginatus* dominates (approximately >90% relative biovolume abundance) until 2.73 Ma, after which *C. radiatus* becomes dominant (Swann et al., 2006; Swann, 2010). Today both *C. marginatus* and *C. radiatus* bloom throughout the year with elevated fluxes in autumn/early winter (Onodera et al., 2005; Takahashi, 1986; Takahashi et al., 1996). Based on this, the previously generated diatom isotope records as well as those obtained in this study are interpreted as reflecting annually averaged conditions with a slight bias toward autumn/early winter months.

Over the analyzed interval, diatom $\delta^{11}B$ ranges from 4.68‰ to 7.20‰, but shifts from a mean of 6.47 ± 0.58 ‰ (± 2σ) between 2.85 - 2.73 Ma, to a mean of 5.58 ± 1.39‰ (± 2σ) between 2.73 - 2.39 Ma ($p < 0.001$) (Fig. 3a). Whilst $\delta^{11}B_{diatom}$ exhibits little variation pre-2.73 Ma, increased variability characterizes the data post-2.73 Ma. $[B]_{diatom}$ ranges from 0.1 ppm to 4.5 ppm and exhibit a marked increase after 2.73 Ma, shifting from a mean of 0.6 ± 1.0 ppm (± 2σ) pre-iNHG, to 2.3 ± 2.1 ppm (± 2σ) post-iNHG ($p < 0.001$) (Fig. 3b). Over the analyzed interval $\delta^{11}B_{diatom}$ and $[B]_{diatom}$ have a negative linear relationship between each other (adjusted $R^2 = 0.41$, $p < 0.001$).

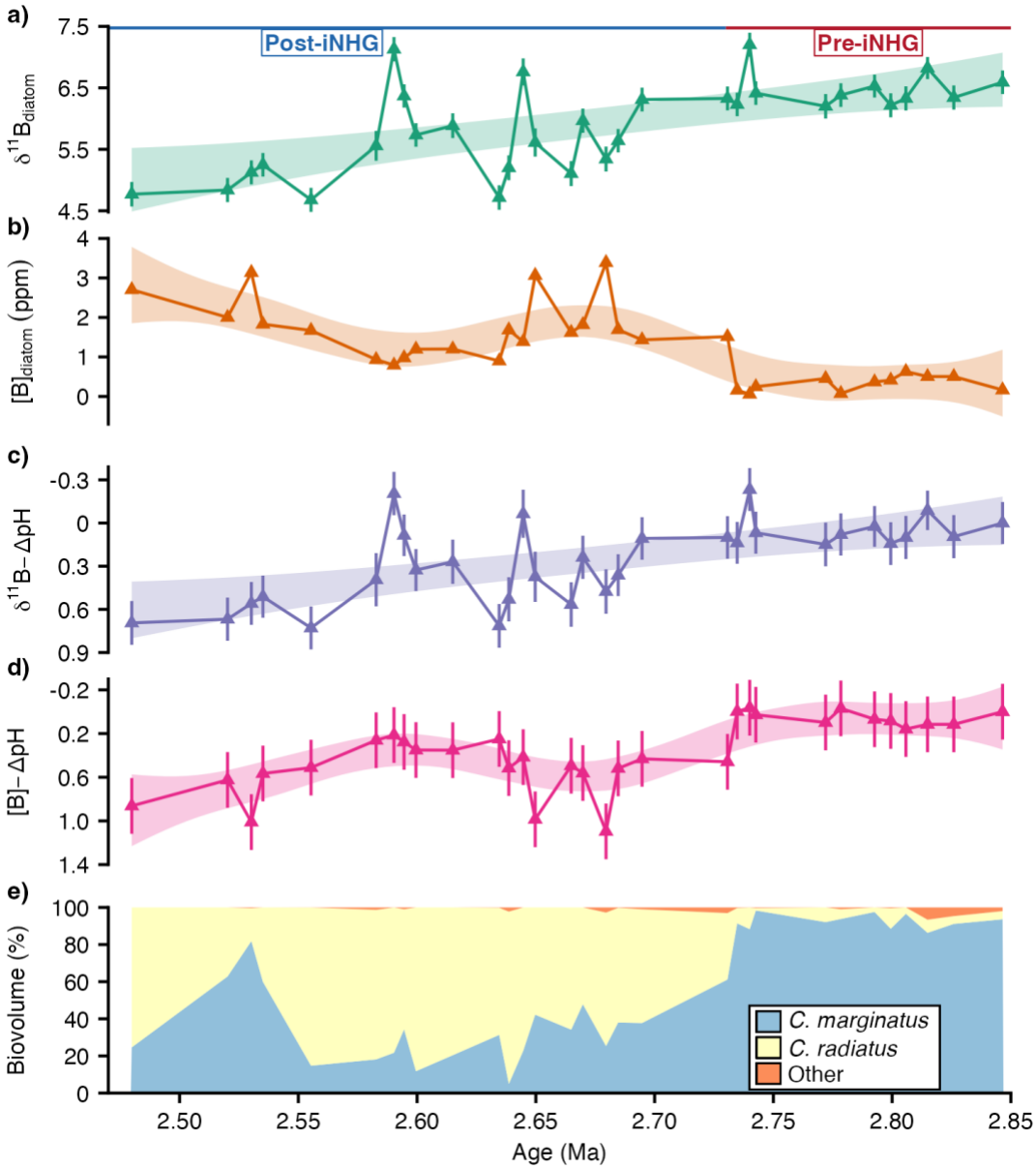

Figure 3. Diatom boron data at ODP Site 882 showing changes in a) $\delta^{11}B_{diatom}$; b) $[B]_{diatom}$; pH relative to a pH of 0 at 2.85 Ma using c) $\delta^{11}B_{diatom}$ ($\delta^{11}B$-ΔpH) and d) $[B]_{diatom}$ ([B]- ΔpH) as well as e) diatom species relative biovolume abundance in the analyzed samples (Swann et al., 2006; Swann, 2010). Shaded regions show the 95% confidence intervals of a generalized

additive models (GAM) fitted to each time series, calculated with restricted maximum likelihood (REML) smoothness selection using the *mgcv* package in R (Wood 2011, 2017; R Core Team, 2024). Red/blue lines at the top of the Figure denote the transition from a pre-iNHG to post-iNHG climate state at 2.73 Ma.3.2 pH reconstruction

A caveat of existing diatom δ^{11}B-pH and [B]-pH calibrations are that they are based on *T. pseudonana* and *T. weissflogii*, rather than the *C. marginatus* and *C. radiatus* taxa found at ODP Site 882. With $\delta^{11}B_{diatom}$ values for the cultured *T. weissflogii* (ca. −2‰ to −6‰) lower than both our bulk diatom in-house standard TC460 and the *C. marginatus*/*C. radiatus* dominated samples in this study (ca. 5‰ to 7‰), further calibrations for different diatom species are required before the diatom δ^{11}B-pH proxy can be rigorously applied. This is particularly important as no study has yet quantified the isotope vital effect (i.e., non-equilibrium isotope fractionation) that may exist between individual taxa. Despite this, $\delta^{11}B_{diatom}$ in both cultured diatom (Donald et al., 2020 - adjusted $R^2 = 0.27$, $p = 0.26$)) and fossilized *C. marginatus*/*C. radiatus* (this study - adjusted $R^2 = 0.41$, $p = <0.01$)) show a negative, albeit uncertain, relationship with [B] (Fig. 4), suggesting a similar mechanism of boron uptake and δ^{11}B-pH relationship for all taxa. For the relationship between $[B]_{diatom}$ and pH, Mejía et al (2013) showed that two species of the same genus also displayed similar $[B]_{diatom}$ concentration in culture. Whilst a direct quantitative reconstruction of pH at ODP Site 882 using the boron based proxies is precluded by the absence of further species-specific calibrations, insights into temporal changes in pH can still be gained by calculating changes relative to the oldest sample at 2.85 Ma (ΔpH) and by assuming that the sensitivity of $\delta^{11}B_{diatom}$ and $[B]_{diatom}$ to pH at ODP Site 882 are the same as those of cultured diatoms of different species (Donald et al., 2020). We elect to not use the [B]-pH calibration of Mejía et al (2013) as, although it is based on two species (*T. weissflogii* and *T. pseudonana*) that are of the same genus to those analyzed in Donald et al. (2020), boron concentrations are 2-3 times higher in Mejía et al (2013). The reasons for this are unknown, but could be due to (i) differences in analytical methods; (ii) differences in cleaning methods; and/or (iii) differences in culturing methodology. By using the Donald et al. (2020) calibration we ensure that there is analytical consistency between the fossilised diatoms and diatoms that form the calibration to reconstruct pH in this study.

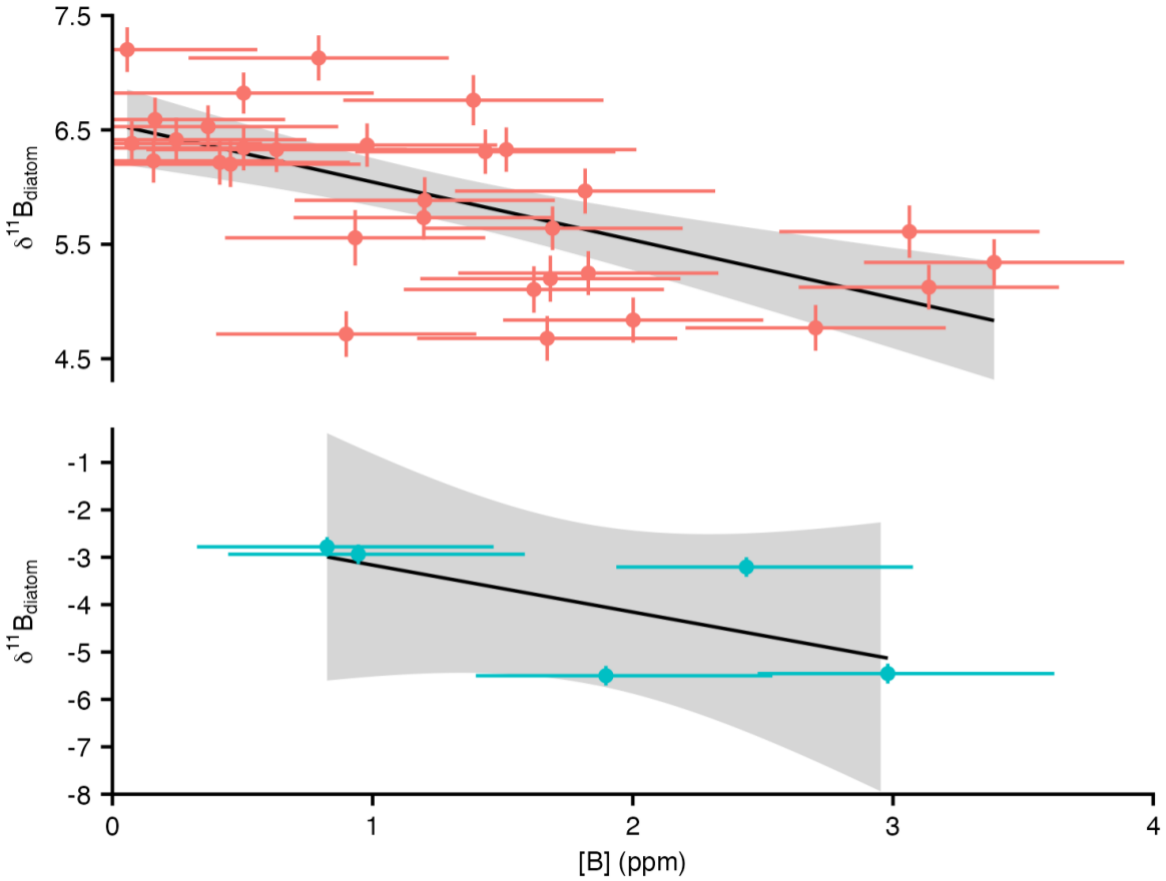

Figure 4. Relationship between $\delta^{11}B$ and [B] in cultured (*T. weissflogii* blue - Donald et al., 2020) and ODP Site 882 (red - this study) diatoms. Black line and shaded regions shows an ordinary least squares linear regression model and associated 95% confidence intervals fitted to each dataset.

Applying the relationship between $\delta^{11}B$ and pH of *T. weissflogii* from Donald et al. (2020), which shows a negative relationship between $\delta^{11}B_{diatom}$ and pH, reveals a trend towards an increase in pH from 2.85 to 2.52 Ma, with a significant increase in both pH and pH variability after 2.73 Ma ($p < 0.001$) (Fig. 3c). This is supported by [B]-ΔpH calculated from the *T. weissflogii* relationship in Donald et al. (2020), in which a significant increase in pH is also observed from 2.73 Ma ($p < 0.001$) (Fig. 3d). Changes in the diatom relative biovolume abundance in the analyzed samples are not strongly associated with either $\delta^{11}B$-ΔpH (adjusted $R^2 = 0.19$, $p = 0.02$) or [B]-ΔpH (adjusted $R^2 = 0.22$, $p = 0.01$) (Fig. 3e; Fig. S2). The weak association that does exist is driven by the major change in *C. marginatus*/*C. radiatus* biovolumes at 2.73 Ma (Fig. 3e), which coincides with broader shifts in the diatom community linked to the cessation of nutrient rich conditions at ODP Site 882 (Shimada et al., 2009). Consequently, we suggest that any apparent link between pH and diatom biovolumes reflects the common response of the diatom community and pH to regional paleoceanographic changes rather than an inter-species vital effect.

4 Discussion

4.1 Carbon dynamics over the iNHG

A reduction in $pCO_{2(atm)}$ is believed to be critical in driving the iNHG (Lunt et al., 2008) with proxy records indicating that concentrations decreased by 40–90 µatm from 2.9-2.7 Ma (Martínez-Botí et al., 2015). Past work has focused on the role of the Southern Ocean in reducing $pCO_{2(atm)}$ over the iNHG, a region which also played a key role in lowering $pCO_{2(atm)}$ by ca. 80-100 ppm over Late Pleistocene glacial-interglacial cycles (Sigman et al., 2021). Key Southern Ocean processes for $pCO_{2(atm)}$ reduction over the iNHG include reduced upwelling of carbon-rich waters, increased Fe fertilization, and reduction in outgassing via sea ice expansion and/or changes in surface ocean circulation (Hodell & Venz-Curtis, 2006; McKay et al., 2012; Naish et al., 2009; Waddell et al., 2009; Martínez-Garcia et al., 2011). The North Pacific has been thought to play a supporting role in the $pCO_{2(atm)}$ decline, via reduced delivery of carbon to the ocean surface (Haug et al., 1999), yet to date such inferences have been based primarily on nutrient proxies (e.g. Sigman et al. 2004).

Based on the mean ΔpH of samples before and after 2.73 Ma, the magnitude of pH change at ODP Site 882 over the iNHG is 0.31 pH units for $\delta^{11}B_{diatom}$ and 0.47 pH units for $[B]_{diatom}$ (Fig. 5). Evidence of a large increase in pH at ODP Site 882 over the iNHG agrees with the hypothesis that the subarctic Pacific Ocean also contributed to global climatic change through this interval by isolating CO_2 in the deep ocean (Haug et al., 1999). The increase in pH at 2.73 Ma is also consistent with $\delta^{13}C_{diatom}$ data, which indicate a decrease in surface water pCO_2 (Fig. 5) (Swann et al., 2018), though we note the need for further calibrations and better understanding of diatom carbon concentrating mechanisms to refine $\delta^{13}C_{diatom}$ reconstructions of pCO_2 (Swann et al., 2018; see Supporting Information).

The pH increase of 0.3-0.5 pH units at ODP Site 882 is considerably greater than that seen in foraminiferal $\delta^{11}B$ from subtropical regions in equilibrium with the atmosphere over the iNHG (Martínez-Botí et al., 2015). This suggests that the subarctic Pacific experienced substantial regional changes in the circulation and biogeochemical processes that govern carbon and nutrient delivery into surface waters, over and above the corresponding global decline in $pCO_{2(atm)}$. It also indicates the ability for oceanographic, nutrient and carbon cycle changes in the subarctic Pacific to have a global impact across a range of timescales, reinforced by evidence that dynamic changes in circulation over the last deglaciation also led to substantial changes in surface water pH and pCO_2 (Gray et al., 2018). Since the 1970s CE $pCO_{2(aq)}$ in the subarctic Pacific has risen broadly in line with $pCO_{2(atm)}$, with annual mean ΔpCO_2 close to 0 µatm (Takahashi et al., 2006, 2009, 2014). If conditions in the Pliocene prior to the iNHG are analogous to those in the future in a warmer climate system (Tierney et al 2019; McClymont et al., 2020), a state with lower pH and higher $pCO_{2(aq)}$ is a plausible mode of 21st Century future variability, with the subarctic Pacific Ocean becoming an increasing net source of atmospheric CO_2 (or weaker CO_2 sink).

336

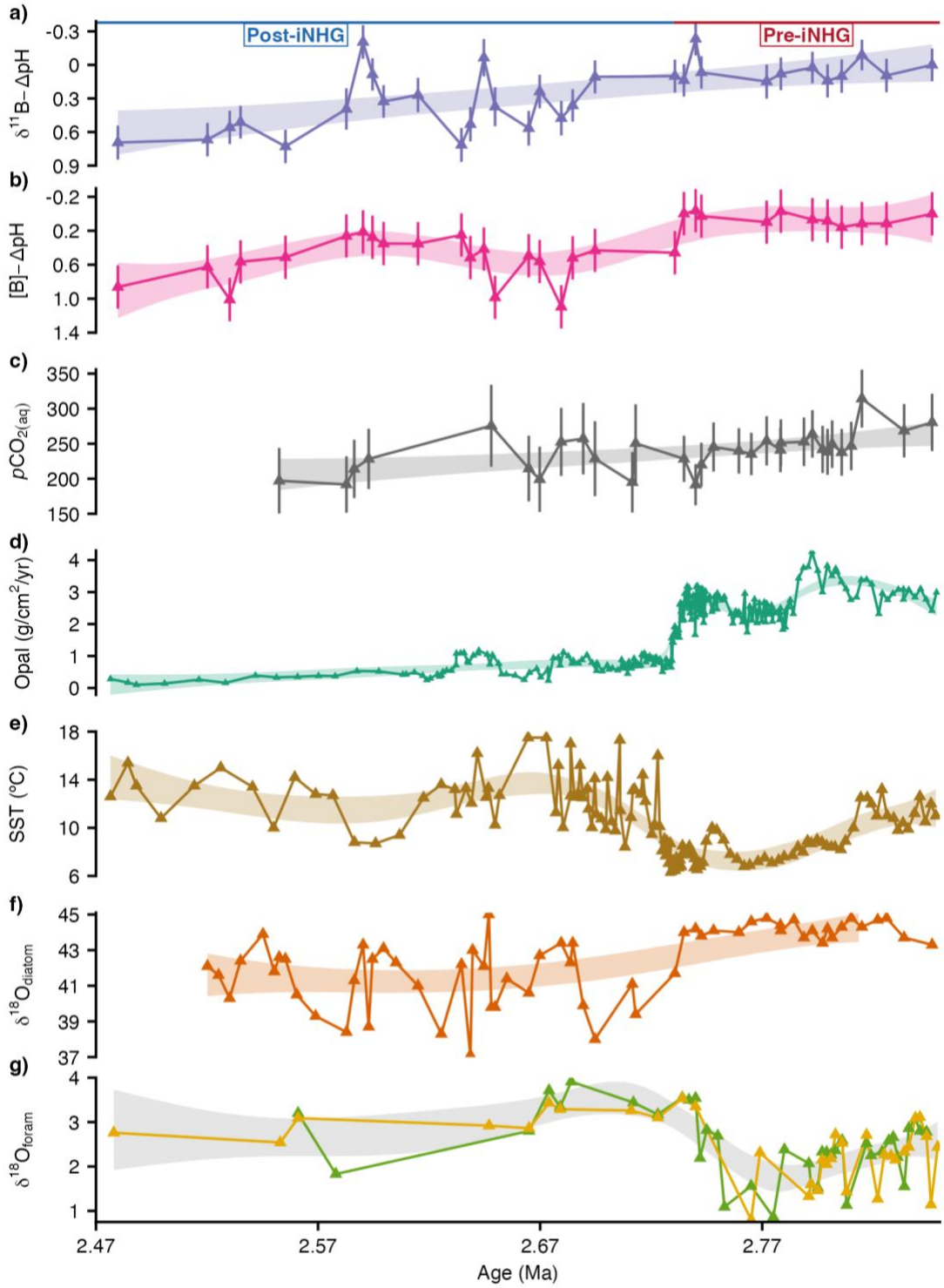

337 **Figure 5.** Paleoceanographic data from ODP Site 882 showing a) δ^{11}B-ΔpH; b) [B]-ΔpH; c)
338 surface water pCO_2 reconstructed from $\delta^{13}C_{diatom}$ (Swann et al., 2018); d) biogenic opal MAR
339 (Haug et al., 1999); e) SST calculated from U^{k}_{37} (Haug et al., 2005); f) diatom δ^{18}O (Swann et

al., 2006; Swann 2010); and g) planktonic foraminifera $\delta^{18}O$ from *Globigerina bulloides* (green) and *Neogloboquadrina pachyderma* (dextral) (yellow) respectively (Maslin et al., 1996, 1998). Shaded regions show the 95% confidence intervals of GAMs fitted to each time series, calculated with restricted maximum likelihood (REML) smoothness selection using the mgcv package in R (Wood 2011, 2017; R Core Team, 2024). Red/blue lines at the top of the Figure denote the transition from a pre-iNHG to post-iNHG climate state at 2.73 Ma.

4.2 Mechanisms for reduced carbon and nutrient delivery

The nature of the circulation and biogeochemical changes in the North Pacific that are recorded by shifts in nutrient and carbon proxies over the iNHG – and also during the Pleistocene – has been a topic of substantial recent discussion (e.g. Burls et al., 2017; Rae et al., 2020; Ford et al., 2022; Abell et al., 2023; Abell and Winckler 2023). The dominant paradigm for the decrease in nutrient delivery over the iNHG has been a regime shift from one with an active Pacific Meridional Overturning Circulation (PMOC), to a more stratified basin with a pronounced, permanent halocline, as seen in the North Pacific today (e.g. Haug et al., 1999, 2005; Burls et al. 2017). Following this paradigm, one interpretation of the pH increase recorded by our data would be that the establishment of stratification at the iNHG reduces carbon delivery to surface waters, increasing pH. A key challenge to this interpretation is that pH today is substantially lower in the stratified subarctic Pacific Ocean than in the vigorously ventilated North Atlantic Ocean (Figure 1), due to the importance of subsurface carbon and nutrient content in controlling carbon and nutrient delivery into surface waters. Although there is substantial convective mixing in the modern North Atlantic Ocean, the subsurface waters brought to the surface by this process have low carbon and nutrient concentrations, due to the flushing of low carbon and nutrient waters from the subtropical gyre through the high latitudes and to depth by an active overturning circulation; this net downwelling means that the North Atlantic is well ventilated and carbon and nutrient poor. In contrast, the lack of overturning circulation in the modern North Pacific allows for the accumulation of extremely carbon- and nutrient-rich waters in the subsurface, and although convective mixing is limited, these waters are still upwelled to the surface by Ekman suction and also delivered via mixing from tidal processes and winter storms (e.g. Sarmiento et al., 2004). The net result is that carbon delivery is higher - and pH lower - in the surface of the subarctic Pacific, which is highly stratified, than in the North Atlantic, which has an active overturning circulation. These observable modern dynamics suggest that stratification alone may not be sufficient to drive the pH change we observe.

Given this modern framework, the increase in pH and decrease in nutrients in the subarctic Pacific Ocean from the iNHG onwards could instead be interpreted as the result of increased ventilation (i.e. a more Atlantic-like regime with net downwelling), where a more active overturning circulation flushes low carbon and nutrient water from the subtropics through the upper water column and to depth, analogous to that proposed for subarctic Pacific Ocean during the Last Glacial Maximum (LGM) by Rae et al. (2020). Prior to the iNHG, the higher than modern opal and excess barium mass accumulation rates could then potentially be explained by the combination of a modern-like state, with potent nutrient and carbon concentrations in the subsurface, and a shift in wind stress (e.g. Abell et al., 2021) which could more efficiently upwell this water into the surface. This is conceptually similar to the model proposed by Gray et

al. (2018) for the Bolling-Allerod period of the last deglaciation, which has comparable opal mass accumulation rates to the pre-iNHG Pliocene, resulting from a stratified water column and enhanced wind-driven upwelling.

A useful test of these interpretations would be reconstructions of ocean ventilation in the upper water column. These are relatively abundant for the LGM, where radiocarbon, redox, and $\delta^{13}C$ data suggest better ventilation of the top 2,000 m of the North Pacific compared to the modern stratified state (e.g. Keigwin, 1998; Rae et al., 2020; Rafter et al., 2022); this ventilated mode is associated with lower nutrient supply to the surface, as outlined above. Ventilation tracers from the iNHG are less abundant. Ford et al. (2022) increased the spatial and depth resolution of carbon isotope data in the Pacific in the Pliocene prior to the iNHG, but there is only one North Pacific site in the upper 2000 m of the water column (which would be most sensitive to changes in North Pacific derived ventilation), and this shows a minor decrease in $\delta^{13}C$ compared to core top values, the opposite of what is predicted in model simulations with an active PMOC (Rae et al., 2020; Ford et al., 2022). Additional data exist at sites below 2,200 m (Burls et al., 2017; Ford et al., 2022), but these may be influenced by deep waters sourced from the Southern Ocean and so their signals cannot be unambiguously attributed to changes in North Pacific ventilation.

Recently, Novak et al. (2024) increased the spatial and temporal resolution of $\delta^{13}C$ data in the pre-iNHG North Pacific. These data show that the mid Pliocene Pacific Ocean is characterized by a systematic decrease in $\delta^{13}C$ from south to north and deep to mid-depth waters. This pattern indicates a mid-Pliocene circulation pattern similar to modern, with waters accumulating respired carbon as they flow from south to north and gradually upwell to shallower depths. This is the opposite of the pattern expected from model simulations with an active deep PMOC (Burls et al., 2017; Ford et al., 2022), leading Novak et al. (2024) to suggest that this mode of circulation is unlikely to have characterized the pre-iNHG North Pacific, thereby arguing against the ventilation to stratification hypothesis, although increased data coverage from shallower depths and over the iNHG itself would allow improved testing of this.

Tracers of surface ocean hydrography may also inform the interpretation of changes in Pacific circulation at the iNHG. Haug et al. (2005) showed that the iNHG is associated with warming SST in the subarctic Pacific, which they attribute to increased seasonality in a more stratified water column (Fig. 5). Alternatively, this could be interpreted as the result of enhanced overturning circulation, consistent with the interpretation of warming in the LGM North Pacific being the result of enhanced glacial PMOC (Rae et al., 2020). Diatom $\delta^{18}O$ shows a decrease over the iNHG (Swann et al., 2006; Swann 2010), implying a reduced salinity, but this signal is not seen in $\delta^{18}O$ in planktic foraminifera from the same core (Maslin et al., 1996, 1998) (Fig. 5).

Finally, model simulations can guide interpretations. In the PlioMIP2 ensemble, the pre iNHG North Pacific experiences consistently higher P-E (precipitation minus evaporation) (Han et al., 2021), leading to surface freshening and a more enhanced halocline compared to modern conditions (Weiffenbach et al., 2023). This is consistent with an enhanced North Pacific halocline under future warming scenarios, and at odds with an enhanced pre-iNHG PMOC. A notable exception to the PlioMIP2 ensemble are the simulations of Burls et al. (2017), in which modification of cloud albedo induces changes in meridional temperature gradients and moisture transport, which lead to increased salinity and enhanced PMOC before the iNHG.

In summary, there are two alternative explanations for North Pacific proxy signals over the iNHG through which the increase in surface ocean pH recorded by our data may be interpreted. The "ventilation to stratification" paradigm for the iNHG has a substantial body of literature support, but would be opposite in sense to modern analogues in the North Atlantic and Pacific Ocean and to the coupled change in circulation and nutrients in the North Pacific at the LGM (Rae et al., 2020). It is also opposite to results from the majority of climate models, which tend to freshen the North Pacific under warmer, Pliocene-like, conditions (Weiffenbach et al., 2023), and recent carbon isotope data (Novak et al., 2024), which argue against PMOC conditions in the Pliocene. The alternative "stratification to ventilation" hypothesis would be consistent with modern analogues, modes of oceanographic variability in the Pleistocene, and better aligned with climate models and new $\delta^{13}C$ data (Novak et al., 2024), but has not yet been much explored in the literature, and may require additional changes in wind-driven upwelling to explain the very high export fluxes of the pre-iNHG Pliocene (see discussion in Abell et al., 2023 and Gray et al., 2018). We encourage future paleo data reconstructions and modelling to try and resolve the nature of these major changes in biogeochemistry and ocean circulation, which our new boron-based data show had significant impact on the carbon cycle.

5 Conclusions

Results from this first down-core record of $\delta^{11}B_{diatom}$ and $[B]_{diatom}$ reveal a major increase in the pH of the subarctic Pacific Ocean over the iNHG, coinciding with a decrease in atmospheric pCO_2 (Martínez-Botí et al., 2015). Based on the magnitude of the increase (0.3 to 0.5 pH units) our findings indicate that this change in the North Pacific may have contributed to the atmospheric CO_2 drawdown, and in turn the global cooling and expansion of large ice-sheets across the Northern Hemisphere through this interval.

Work in this current study and others cited within has shown that profound shifts in regional biogeochemistry are possible under altered climate conditions, with the potential to significantly alter carbon dynamics including ΔpCO_2 and the outgassing of CO_2 to the atmosphere. If Pliocene pre-iNHG conditions are an analogue of future climate change, then increased regional acidification and outgassing may occur over the course of the 21st century.

Acknowledgments

HKD and GLF wish to thank J. Andy Milton for support with mass spectrometry and Agnes Michalik and Mathew Cooper for clean laboratory assistance. This research was supported by a Natural Environmental Research Council (NERC, UK) studentship to HKD NE/L002531/1) and NERC standards grant NE/J021075/1 to GLF.

Open Research

Supporting data ($\delta^{11}B_{diatom}$, $[B]_{diatom}$ and reconstructed pH data used in this study) are included as a spreadsheet in the SI. The data has also been deposited in Pangaea (www.pangaea.de) at

https://doi.org/10.1594/PANGAEA.971873 (Donald et al., 2024) and will be made publicly available when the article is accepted for publication.

References

Abell, J. T., & Winckler, G. (2023). Long-term variability in Pliocene North Pacific Ocean export production and its implications for ocean circulation in a warmer world. *AGU Advances*, 4, e2022AV000853.

Abell, J. T., Winckler, G., Anderson, R. F. & Herbert, T. D. (2021) Poleward and weakened westerlies during Pliocene warmth. *Nature*, 589, 70–75.

Abell, J. T., Winckler, G., Pullen, A., Kinsley, C. W., Kapp, P. A., Middleton, J. L., Pavia, F. J., McGee, D., Ford, H. L. & Raymo, M. E. (2023). Evaluating the drivers of Quaternary dust fluxes to the western North Pacific: East Asian dustiness and Northern Hemisphere gustiness. *Paleoceanography and Paleoclimatology*, 38, e2022PA004571.

Badger, M. P. S., Chalk, T. B., Foster, G. L., Bown, P. R., Gibbs, S. J., Sexton, P. F., Schmidt, D. N., Pälike, H., Mackensen, A., & Pancost, R. D. (2019). Insensitivity of alkenone carbon isotopes to atmospheric CO_2 at low to moderate CO_2 levels, *Climate of the Past*, 15, 539-554.

Bailey, I., Liu, Q., Swann, G. E. A., Jiang, Z., Sun, Y., Zhao, X., & Roberts, A. P. (2011). Iron fertilisation and biogeochemical cycles in the sub-Arctic Northwest Pacific during the late Pliocene intensification of northern hemisphere glaciation. *Earth and Planetary Science Letters*, 307, 253-265.

Brierley, C. M., & Fedorov, A. V. (2010). Relative importance of meridional and zonal sea surface temperature gradients for the onset of the ice ages and Pliocene-Pleistocene climate evolution. *Paleoceanography*, 25, PA2214.

Burls, N. J,. Fedorov, A. V., Sigman, D. M., Jaccard, S. L., Tiedemann, R., & Haug, G. H. (2017). Active Pacific meridional overturning circulation (PMOC) during the warm Pliocene. *Science Advances*, 3, e1700156.

Catanzaro E. J., Champion C. E., Garner E. L., Marinenko G., Sappenfield K. M., & Shields W. R. (1970). *Boric Acid: Isotopic and Assay Standard Reference Materials*, National Bureau of Standards Special Publications: Institute for Materials Research, Washington, D. C.

Chalk, T. B., Hain, M. P., Foster, G. L., Rohling, E. J., Sexton, P. F., Badger, M. P. S., Cherry, S. G., Hasenfratz, A. P., Haug, G. H., Jaccard, S. L., Martínez-Garcia, A., Pälike, H., Pancost, R. D., & Wilson, P. A. (2017). *Causes of ice age intensification across the Mid-Pleistocene Transition. Proceedings of the National Academy of Sciences of the United States of America*, 114, 201702143.

CenCO$_2$PIP Consortium. (2023). Toward a Cenozoic history of atmospheric CO_2. *Science*, 382, eadi5177.

Donald, H. K., Foster, G. L., Fröhberg, B., Swann, G. E. A., Poulton, A. J., Moore, C. M., & Humphreys, M. P. (2020). The pH dependency of the boron isotopic composition of diatom opal (*Thalassiosira weissflogii*). *Biogeosciences*, 17, 2825–2837.

Donald, H. K., Swann, G. E. A., Rae, J. W. B., & Foster, G. L. (2024): Diatom boron isotope data from ODP Site 882 over the intensification of Northern Hemisphere Glaciation [dataset]. PANGAEA, https://doi.org/10.1594/PANGAEA.971873.

Ford, H. L., Burls, N. J., Jacobs, P., Jahn, A., Caballero-Gill, R. P., Hodell, D. A., & Fedorov, A. V. (2022). Sustained mid-Pliocene warmth led to deep water formation in the North Pacific. *Nature Geoscience*, 15, 658-663.

Foster G. L. (2008) Seawater pH, *p*CO2 and [CO3]2 variations in the Caribbean Sea over the last 130 kyr: A boron isotope and B/Ca study of planktic foraminifera. *Earth and Planetary Science Letters*, 271, 254-266.

Foster G. L., Pogge von Strandmann P. A. E. & Rae J. W. B. (2010). Boron and magnesium isotopic composition of seawater. *Geochemistry, Geophysics. Geosystems*, 11, 1-10.

Foster G. L., & Rae J. W. B. (2016). Reconstructing ocean pH with boron isotopes in foraminifera. Annu. Rev. *Earth and Planetary Science Letters*. 44, 207-237.

Galbraith, E. D., M. Kienast, S. L. Jaccard, T. F. Pedersen, B. G. Brunelle, D. M. Sigman, and T. Kiefer (2008). Consistent relationship between global climate and surface nitrate utilization in the western subarctic Pacific throughout the last 500 ka. *Paleoceanography*, 23, PA2212.

Gray, W. R., Rae, J. W. B., Wills, R. C. J., Shevenell, A. E., Taylor, B., Burke, A., Foster, G. L., & Lear, C. (2018). Deglacial upwelling, productivity and CO_2 outgassing in the North Pacific Ocean. *Nature Geoscience*. 11, 340-344.

Han, Z., Zhang, Q., Li, Q., Feng, R., Haywood, A. M., Tindall, J. C., Hunter, S. J., Otto-Bliesner, B. L., Brady, E. C., Rosenbloom, N., Zhang, Z, Li, X., Guo, C., Nisancioglu, K. H., Stepanek, C., Lohmann, G., Sohl, L. E., Chandler, M. A., Tan, N., Ramstein, G., Baatsen, M. L. J., von der Heydt, A. S., Chandan, D., Peltier, W. R., Williams, C. J. R., Lunt, D. J., Cheng, J., Wen, Q., & Burls, N. J. (2021). Evaluating the large-scale hydrological cycle response within the Pliocene Model Intercomparison Project Phase 2 (PlioMIP2) ensemble. *Climate of the Past*, 17, 2537–2558.

Haug, G. H., Maslin, M. A., Sarnthein, M., Stax, R., Tiedemann R., (1995) Evolution of Northwest Pacific Sedimentation Patterns since 6 MA (Site 882). In D. K. Rea, I. A. Basov, D. W. Scholl, & J. F. Allan (Eds.), Proceedings of the Ocean Drilling Program, Scientific Results Volume (pp. 293–314). College Station, TX: Ocean Drilling Program.

Haug, G. H., Sigman, D. M., Tiedemann, R., Pedersen, T. F., & Sarnthein, M. (1999). Onset of permanent stratification in the subarctic Pacific Ocean. *Nature*, 401, 779-782.

Haug, G. H., Ganopolski, A., Sigman, D. M., Rosell-Mele, A., Swann, G. E. A., Tiedemann, R., Jaccard, S., Bollmann, J., Maslin, M. A., Leng, M. J., & Eglinton, G. (2005). North Pacific seasonality and the glaciation of North America 2.7 million years ago. *Nature*. 433, 821-825.

Hemming, N. G., & Hanson, G. N. (1992). Boron isotopic composition and concentration in modern marine carbonates. *Geochimica et Cosmochimica Acta*, 56, 537-543.

Henehan, M. J., Rae, J. W. B., Foster, G. L., Erez, J., Prentice, K. C., Kucera, M., Bostock, H. C., Martínez-Botí, M. A., Milton, J. A., Wilson, P. A., Marshall, B. J. & Elliott, T. (2013) Calibration of the boron isotope proxy in the planktonic foraminifera *Globigerinoides ruber* for use in palaeo-CO_2 reconstruction. *Earth and Planetary Science Letters*. 364, 111-122.

Hendry, K. R. & Andersen, M. B. (2013). The zinc isotopic composition of siliceous marine sponges: Investigating nature's sediment traps. *Chemical Geology*, 354, 33-41.

Hodell, D. A., & Venz-Curtis, K. A. (2006). Late Neogene history of deepwater ventilation in the Southern Ocean. *Geochemistry, Geophysics, Geosystems*, 7, Q09001.

Hönisch, B., & Hemming, N. G. (2005) Surface ocean pH response to variations in pCO_2 through two full glacial cycles. *Earth and Planetary Science Letters*. 236, 305-314.

Hönisch, B., Eggins, S., Haynes, L., Allen, K., Holland, K., & Lorbacher, K. (2019). Boron Proxies in Paleoceanography and Paleoclimatology. Wiley-Blackwell.

Horn M. G., Robinson R. S., Rynearson T. A., & Sigman D. M. (2011) Nitrogen isotopic relationship between diatom-bound and bulk organic matter of cultured polar diatoms. *Paleoceanography*, 26, PA3208.

Ishikawa, T., & Nakamura E. (1993). Boron isotope systematics of marine sediments. *Earth and Planetary Science Letters*. 117, 567-580.

Japan Agency for Marine-Earth Science and Technology; Atmosphere and Ocean Research Institute; Centre for Climate System Research-National Institute for Environmental Studies (2013): WCRP CMIP5: The MIROC team MIROC-ESM model output collection. Centre for Environmental Data Analysis, 26th February 2018. Retrieved from http://catalogue.ceda.ac.uk/uuid/bf3c7e63092b45f2927e3e1d260c4f01

Keigwin, L. D. (1998), Glacial-age hydrography of the far northwest Pacific Ocean, *Paleoceanography*, 13, 323-339.

Kleiven, H. F., Jansen, E., Fronval, T., & Smith, T. M. (2002). Intensification of Northern Hemisphere glaciations in the circum Atlantic region (3.5–2.4 Ma) – ice-rafted detritus evidence. *Palaeogeography, Palaeoclimatology, Palaeoecology*, 184, 213-223.

Klochko, K., Kaufman, A.J., Yao, W., Byrne, R.H., Tossell, J.A. (2006). Experimental measurement of boron isotope fractionation in seawater. *Earth and Planetary Science Letters*. 248, 276-285.

Kolodny, Y., & Chaussidon, M. (2004). Boron isotopes in DSDP cherts: Fractionation and diagenesis. *The Geochemical Society Special Publications*, 9, 1-14.

Lemarchand, D., Gaillardet, J., Gopel, C. & Manhes G. (2002). An optimized procedure for boron separation and mass spectrometry analysis for river samples. *Chemical Geology*, 182, 323-334.

Locarnini, R. A., Mishonov, A. V., Baranova, O. K., Boyer, T. P., Zweng, M. M., Garcia, H. E., Reagan, J. R., Seidov, D., Weathers, K., Paver, C. R., & Smolyar, I. (2018). World Ocean

Atlas 2018, Volume 1: Temperature. A. Mishonov Technical Ed.; NOAA Atlas NESDIS 81, 52pp.

Lunt, D. J., Foster, G. L., Haywood, A. M., & Stone, E. J. (2008). Late Pliocene Greenland glaciation controlled by a decline in atmospheric CO_2 levels. *Nature*, 454, 1102–1105.

Martínez-Botí M. A., Foster, G. L., Chalk, T. B., Rohling, E. J., Sexton, P. F., Lunt, D. J., Pancost, R.D., Badger, M.P.S., & Schmidt, D.N. (2015). Plio-Pleistocene climate sensitivity evaluated using high-resolution CO_2 records. *Nature*, 518, 49-54.

Martínez-Garcia, A., Rosell-Melé, A., Jaccard, S. L., Geibert, W., Sigman, D. M., & Haug, G. H. (2011). Southern Ocean dust–climate coupling over the past four million years. *Nature*, 476, 312-315.

Maslin, M. A., Haug, G. H., Sarnthein, M., & Tiedemann, R. (1996). The progressive intensification of northern hemisphere glaciation as seen from the North Pacific. *Geologische Rundschau*, 85, 452–465.

Maslin, M. A., Li, X. S., Loutre, M. -F., & Berger, A. (1998) The contribution of orbital forcing to the progressive intensification of Northern Hemisphere Glaciation. *Quaternary Science Reviews*, 17, 411-426.

McClymont, E. L., Ford, H. L., Ho, S. L., Tindall, J. C., Haywood, A. M., Alonso-Garcia, M., Bailey, I., Berke, M. A., Littler, K., Patterson, M. O., Petrick, B., Peterse, F., Ravelo, A.C., Risebrobakken, B., De Schepper, S., Swann, G.E.A., Thirumalai, K., Tierney, J.E., van der Weijst, C., White, S., Abe-Ouchi, A., Baatsen, M.L.J., Brady, E.C., Chan, W.-L., Chandan, D., Feng, R., Guo, C., von der Heydt, A.S., Hunter, S., Li, X., Lohmann, G., Nisancioglu, K.H., Otto-Bliesner, B.L., Peltier, W.R., Stepanek, C., & Zhang, Z. (2020). Lessons from a high-CO_2 world: an ocean view from ~3 million years ago. *Climate of the Past*, 16, 1599-1615.

McClymont, E. L., Ho, S. L., Ford, H. L., Bailey, I., Berke, M. A., Bolton, C. T., De Schepper, S., Grant, G. R., Groeneveld, J., Inglis, G. N., Karas, C., Patterson, M. O., Swann, G. E. A., Thirumalai, K., White, S. M., Alonso-Garcia, M., Anand P., Hoogakker, B. A. A., Littler, K., Petrick, B. F., Risebrobakken, B., Abell, J. T., Crocker, A. J., de Graaf, F., Feakins S. J., Hargreaves, J. C., Jones, C. L., Markowska, M., Ratnayake, A. S., Stepanek, C., & Tangunan, D. (2023). Climate evolution through the onset and intensification of Northern Hemisphere Glaciation. *Reviews of Geophysics*, 61, e2022RG000793.

McKay, R., Naish, T., Carter, L., Riesselman, C., Dunbar, R., Sjunneskog, C., Winter, D., Sangiorgi, F., Warren, C., Pagani, M., Schouten, S., Willmott, V., Levy, R., DeConto, R., & Powell, R.D. (2012). Antarctic and Southern Ocean influences on Late Pliocene global cooling. *Proceedings of the National Academy of Sciences of the United States of America*, 109, 6423-6428.

Meinshausen, M., Nicholls, Z. R. J., Lewis, J., Gidden, M. J., Vogel, E., Freund, M., Beyerle, U., Gessner, C., Nauels, A., Bauer, N., Canadell, J. G., Daniel, J. S., John, A., Krummel, P. B., Luderer, G., Meinshausen, N., Montzka, S. A., Rayner, P. J., Reimann, S., Smith, S. J., van den Berg, M., Velders, G. J. M., Vollmer, M. K., & Wang, R. H. J. (2020). The shared socio-economic pathway (SSP) greenhouse gas concentrations and their extensions to 2500. *Geoscientific Model Development*. 13, 3571-3605.

Mejía, L. M., Isensee K., Méndez-Vicente A., Pisonero J., Shimizu N., Gonz´alez C., Monteleone B. & Stoll H. (2013). B content and Si/C ratios from cultured diatoms (*Thalassiosira pseudonana* and *Thalassiosira weissflogii*): Relationship to seawater pH and diatom carbon acquisition. *Geochimica et Cosmochimica Acta*,123, 322-337.

Naish, T., Powell, R., Levy, R., Wilson, G., Scherer, R., Talarico, F., Krissek, L., Niessen, F., Pompilio, M., Wilson, T., Carter, L., DeConto, R., Huybers, P., McKay, R., Pollard, D., Ross, J., Winter, D., Barrett, P., Browne, G., Cody, R., Cowan, E., Crampton, J., Dunbar, G., Dunbar, N., Florindo, F., Gebhardt, C., Graham, I., Hannah, M., Hansaraj, D., Harwood, D., Helling, D., Henrys, S., Hinnov, L., Kuhn, G., Kyle, P., Läufer, A, Maffioli, P., Magens, D., Mandernack, K., McIntosh, W., Millan, C., Morin, R., Ohneiser, C., Paulsen, T., Persico, D., Raine, I., Reed, J., Riesselman, C., Sagnotti, L., Schmitt, D., Sjunneskog, C., Strong, P., Taviani, M., Vogel, S., Wilch, T. & Williams, T. (2009). Obliquity-paced Pliocene West Antarctic ice sheet oscillations. *Nature*, 458, 322-328.

Novak, J. B., Caballero-Gill, R. P., Rose, R. M., Herbert, T. D. & Dowsett, H. J. (2024). Isotopic evidence against North Pacific Deep Water formation during late Pliocene warmth. *Nature Geoscience*, 17, 795-802.

Nir, O., Vengosh, A., Harkness, J. S., Dwyer, G. S. & Lahav, O. (2015). Direct measurement of the boron isotope fractionation factor: reducing the uncertainty in reconstructing ocean paleo-pH. *Earth and Planetary Sciences*, 414, 1-5

Olsen, A., Lange, N., Key, R. M., Tanhua, T., Bittig, H. C., Kozyr, A., Àlvarez, M., Azetsu-Scott, K., Becker, S., Brown, P. J., Carter, B. R., Cotrim da Cunha, L., Feely, R. A., van Heuven, S., Hoppema, M., Ishii, M., Jeansson, E., Jutterström, S., Landa, C. S., Lauvset, S. K., Michaelis, P., Murata, A., Pérez, F. F., Pfeil, B., Schirnick, C., Steinfeldt, R., Suzuki, T., Tilbrook, B., Velo, A., Wanninkhof, R. and Woosley, R. J.(2020). GLODAPv2.2020 – the second update of GLODAPv2. . doi:10.5194/essd-12-3653-2020.

Onodera, J., Takahashi, K., & Honda, M. C. (2005). Pelagic and coastal diatom fluxes and the environmental changes in the northwestern North Pacific during December 1997–May 2000. *Deep Sea Research Part II*, 52, 2218-2239.

Pearson P. N. & Palmer M. R. (2000). Atmospheric carbon dioxide concentrations over the past 60 million years. *Nature*, 406, 695-699.

Rae, J. W. B., Gray, W. R., Wills, R. C. J., Eisenman, I., Fitzhugh, B., Fotheringham, M., Littley, E.F.M., Rafter, P.A., Rees-Owen, R., Ridgwell, A., Taylor, B., & Burke, A. (2020). Overturning circulation, nutrient limitation, and warming in the Glacial North Pacific. *Science Advances*, 6: eabd1654.

Rae, J. W. B., Zhang, Y. G., Liu, X., Foster, G. L., Stoll, H. M., & Whiteford, R. D. M. (2021). Atmospheric CO_2 over the past 66 million years from marine archives. *Annual Review of Earth and Planetary Sciences*. 49, 609-641.

Rafter, P. A., Gray, W. R., Hines, S. K., Burke, A., Costa, K. M., Gottschalk, J., Hain, M. P., Rae, J. W., Southon, J. R., Walczak, M. H., & Yu, J. (2022). Global reorganization of deep-sea circulation and carbon storage after the last ice age. *Science Advances*., 8, p.eabq5434.

Reynolds, B. C., Frank, M., & Halliday, A. N. (2008). Evidence for a major change in silicon cycling in the subarctic North Pacific at 2.73 Ma. *Paleoceanography*, 23, PA4219.

Saldi, G. D., Louvat, P., Schott, J., & Gaillardet, J. (2021) The pH dependence of the isotopic composition of boron adsorbed on amorphous silica. *Geochimica et Cosmochimica Acta*, 308, 1-20.

Sarmiento, J. L., Gruber, N., Brezinski, M. A., & Dunne, J. P. (2004). High-latitude controls of thermocline nutrients and low latitude biological productivity. *Nature*. 427, 56-60.

Sato, M., Makio, M., Hayashi, T., & Ohno, M. (2015). Abrupt intensification of North Atlantic Deep Water formation at the Nordic Seas during the late Pliocene climate transition. *Geophysical Research Letters*, 42, 4949-4955.

Shimada, C., Sato, T., Yamasaki, M., Hasegawa, S., & Tanaka, T. (2009). Drastic change in the late Pliocene subarctic Pacific diatom community associated with the onset of the Northern Hemisphere glaciation. *Palaeogeography, Palaeoclimatology, Palaeoecology*, 279, 207-215.

Sigman, D. M., Jaccard, S. L., & Haug, G. H. (2004). Polar ocean stratification in a cold climate. *Nature*, 428, 59-63.

Sigman, D. M., Fripiat, F., Studer, A. S., Kemeny, P. C., Martínez-García, A., Hain, M. P., Ai, X., Wang, X., Ren, H., & Haug, G. H. (2021). The Southern Ocean during the ice ages: A review of the Antarctic surface isolation hypothesis, with comparison to the North Pacific. *Quaternary Science Reviews*, 254, 106732.

Stoll, H. M., Guitian, J., Hernandez-Almeida, I., Mejía, L. M., Phelps, S., Polissar, P., Rosenthal, Y., Zhang, H., & Ziveri, P. (2019). Upregulation of phytoplankton carbon concentrating mechanisms during low CO_2 glacial periods and implications for the phytoplankton pCO_2 proxy. *Quaternary Science Reviews*, 208 1-20.

Studer, A. S., Martínez-Garcia, A., Jaccard, S. L., Girault, F. E., Sigman, D. M., & Haug, G. H. (2012). Enhanced stratification and seasonality in the subarctic Pacific upon Northern Hemisphere glaciation—New evidence from diatom-bound nitrogen isotopes, alkenones and archaeal tetraethers. *Earth and Planetary Science Letters*, 351-352, 84-94.

Swann, G. E. A. (2010). Salinity changes in the North West Pacific Ocean during the late Pliocene/early Quaternary from 2.73 Ma to 2.53 Ma. *Earth and Planetary Science Letters*, 297, 332-338.

Swann, G. E. A., Maslin, M. A., Leng, M. J., Sloane, H. J., & Haug, G. H. (2006). Diatom $\delta^{18}O$ evidence for the development of the modern halocline system in the subarctic northwest Pacific at the onset of major Northern Hemisphere glaciation. *Paleoceanography*, 21, PA1009.

Swann, G. E. A., Kendrick, C. P., Dickson, A. J., & Worne, S. (2018). Late Pliocene marine pCO_2 reconstructions from the subarctic Pacific Ocean. *Paleoceanography and Paleoclimatology*, 33, 457-469.

Takahashi, K. (1986). Seasonal fluxes of pelagic diatoms in the subarctic Pacific, 1982-1983. *Deep Sea Research Part A. Oceanographic Research Papers*, 33, 1225-1251.

Takahashi, K., Hisamichi, K., Yanada, M., & Maita, Y. (1996). Seasonal changes of marine phytoplankton productivity: A sediment trap study (in Japanese). *Kaiyo Monthly*, 10, 109-115.

Takahashi, T., Sutherland, S. C., Feely, R.A., & Wanninkhof, R. (2006). Decadal change of the surface water pCO_2 in the North Pacific: A synthesis of 35 years of observations. *Journal of Geophysical Research*, 111, C07S05.

Takahashi, T., Sutherland, S. C., Wanninkhof, R., Sweeney, C., Feely, R. A., Chipman, D. W., Hales, B., Friederich, G., Chavez, F., Sabine, C., Watson, A., Bakker, D. C. E., Schuster, U., Metzl, N., Yoshikawa-Inoue, I., Ishii, M., Midorikawa, T., Nojiri, Y., Körtzinger, A., Steinhoff, T., Hoppema, M., Olafsson, J., Arnarson, T.S., Tilbrook, B., Johannessen, T., Olsen, A., Bellerby, R., Wong, C. S., Delille, B., Bates, N. R., & de Baar, H.J.W. (2009). Climatological mean and decadal changes in surface ocean pCO_2, and net sea-air CO_2 flux over the global oceans. *Deep Sea Research Part II*, 56, 554-577.

Takahashi T., Sutherland S. C., Chipman D. W., Goddard J. G., and Ho C. (2014) Climatological distributions of pH, pCO_2, total CO_2, alkalinity, and $CaCO_3$ saturation in the global surface ocean, and temporal changes at selected locations. *Marine Chemistry*, 164, 95-125.

Takahashi, T., Sutherland, S. C., & Kozyr, A. (2016). Global ocean surface water partial pressure of CO_2 database: measurements performed during 1957–2015 (2015). ORNL/CDIAC-160, NDP-088(V2015). Carbon Dioxide Information Analysis Center, Oak Ridge National Laboratory, U.S. Department of Energy, Oak Ridge, Tennessee.

Tan, N., Ladant, J. B., Ramstein, G., Dumas, C., Bachem, P., & Jansen, E. (2018). Dynamic Greenland ice sheet driven by pCO_2 variations across the Pliocene Pleistocene transition. *Nature Communications*, 9, 4755.

Thomas, Z. A. (2016). Using natural archives to detect climate and environmental tipping points in the Earth System. *Quaternary Science Reviews*, 152, 60-71.

Tiedemann, R., & Haug, G. H. (1995). Astronomical calibration of cycle stratigraphy for Site 882 in the northwest Pacific. In D. K. Rea, I. A. Basov, D. W. Scholl, & J. F. Allan (Eds.), Proceedings of the Ocean Drilling Program, Scientific Results Volume (pp. 283–292). College Station, TX: Ocean Drilling Program.

Tierney, J. E., Haywood, A. M., Feng, R., Bhattacharya, T., & Otto-Bliesner, B. L. (2019). Pliocene warmth consistent with greenhouse gas forcing. *Geophysical Research Letters*, 46, 9136–9144

Tierney, J. E, Poulsen, C. J, Montañez, I. P, Bhattacharya, T, Feng, R., Ford, H. L., Hönisch, B, Inglis, G. N., Petersen, S. V., Sagoo, N, Tabor, C. R. , Thirumalai, K, Zhu, J., Burls, N. J., Foster, G. L., Goddéris, Y., Huber, B. T. Ivany, L. C., Turner, S. T., Lunt, D. J., McElwain, J. C., Mills, B. J. W., Otto-Bliesner, B. L. , Ridgwell, A., & Zhang, Yi Ge. (2020). Past climates inform our future. *Science*, 370, eaay3701.

Vogl, J., & Rosner, M. (2012). Production and certification of a unique set of isotope and delta reference materials for boron isotope determination in geochemical, envi- ronmental and industrial materials. *Geostandards and Geoanalytical Research*, 36, 161-175.

744 Waddell, L. M., Hendy, I. L., Moore, T. C., & Lyle, M. W. (2009). Ventilation of the abyssal
745 Southern Ocean during the late Neogene: A new perspective from the subantarctic
746 Pacific. *Paleoceanography*, 24, PA3206.

747 Weiffenbach, J. E., Baatsen, M. L. J., Dijkstra, H. A., von der Heydt, A. S., Abe-Ouchi, A.,
748 Brady, E. C., Chan, W. -L., Chandan, D., Chandler, M. A., Contoux, C., Feng, R., Guo,
749 C., Han, Z., Haywood, A. M., Li, Q., Li, X., Lohmann, G., Lunt, D. J., Nisancioglu, K.
750 H., Otto-Bliesner, B. L., Peltier, W. R., Ramstein, G., Sohl, L. E., Stepanek, C., Tan, N.,
751 Tindall, J. C., Williams, C. J. R., Zhang, Q., & Zhang, Z. (2023). Unraveling the
752 mechanisms and implications of a stronger mid-Pliocene Atlantic Meridional
753 Overturning Circulation (AMOC) in PlioMIP2. *Climate of the Past*. 19, 61-85.

754 R Core Team, R: A language and environment for statistical computing. R Foundation for
755 Statistical Computing, Vienna, Austria. https://www.R-project.org/ (2024).

756 Wood, S. N. (2011). Fast stable restricted maximum likelihood and marginal likelihood
757 estimation of semiparametric generalized linear models. *Journal of the Royal Statistical*
758 *Society B*. 73, 3-36.

759 Wood, S. N. (2017). Generalized Additive Models: An Introduction with R. CRC Press.

760 Wunderling, N., Donges, J. F., Kurths, J., & Winkelmann, R. (2021). Interacting tipping
761 elements increase risk of climate domino effects under global warming. *Earth System*
762 *Dynamics*, 12, 601-619.

763 Zeebe, R. E., & Wolf-Gladrow, D. A. (2001). *CO_2 in Seawater: equilibrium, kinetics, isotopes*.
764 Amsterdam: Elsevier.

765 Zweng, M. M., Reagan, J. R., Seidov, D., Boyer, T. P., Locarnini, R. A., Garcia, H. E.,
766 Mishonov, A. V., Baranova, O. K., Weathers, K., Paver, C. R., & Smolyar I, (2018).
767 World Ocean Atlas 2018, Volume 2: Salinity. A. Mishonov Technical Ed.; NOAA Atlas
768 NESDIS 82, 50pp.